

# Motorcycle Tire Crash Analysis

Shigeru Fujii

● Dynamics Department Advanced Technology Research Division

## Abstract

When a motorcycle crashes, the front tire receives the reaction force first. This force influences the following motions of the motorcycle and the rider. The reaction force for the tire should be therefore calculated with considerable accuracy, otherwise the evaluation of injury potential through motorcycle crash simulation may contain serious error. This paper describes the development of an FE model of a tire containing rubber, nylon cord and compressed air, with an aluminum rim. The results of the tire crash simulation using this model were in good agreement with the data from both static and dynamic experiments.

## 1 INTRODUCTION

There are various configurations of crashes between motorcycles and cars. Therefore, the application of simulation models is promising, and some reports showing the usefulness of simulations for motorcycle crash analysis have been published<sup>1,2)</sup> in recent years. On the other hand, there is a large degree of freedom in the possible behavior of the rider in a collision (**Fig. 1**) and the repeatability of that behavior is low. For example, when motorcycles crash into the sides of cars in full scale crash tests, small differences such as whether the front tire of the motorcycle hits the center pillar of the car or not cause large differences in following motion. Consequently, the reaction force of the front tire must be calculated with enough accuracy to simulate such crashes. This paper describes an FE (Finite Element) model of the motorcycle tire that is intended to estimate the reaction force of a tire accurately, including cases where the rim of the wheel is broken.



Fig.1 A crash test between a motorcycle and an automobile

## 2 Analytical model

Generally, wheels are modeled as rigid elements or constraint points in FEM (Finite Element Method) models of tires. However, rims of wheels are sometimes broken in full scale crash tests. To simulate such cases rims were FEM modeled as a deformable element here. Also, the nylon cord component was modeled as several layers of membrane elements that are reinforced in one direction for each layer. The directions were made to coincide with the actual layout of the bias tire which was the object for the model. Tire rubber was modeled as a solid element. Air elements<sup>3)</sup> which were designed to simulate the change of internal pressure were placed around the periphery of the enclosed area covered by the tire and rim (Fig. 2, 3).

### 2.1. Modeling of the rim and its periphery

For the wheel, only the rim was modeled, and the base of the rim was modeled as a constraint point along its full circumference (Fig. 3). Analysis results did not show significant differences in the case of a model created to simulate spoked wheels.

Therefore, the modeling of spokes was eliminated to shorten analysis time.

As the areas surrounded by ellipses in Fig. 3 are pressed tightly against the rim by means of bead wires, common nodes were used for the rim and tire. On the other hand, the area between the rim and sidewall of the tire was modeled as a contact boundary because it can slip on impact. Because there is severe deformation of the sidewall around the tips of the rim, a finer mesh size was necessary for this area of the tire. The material data for the rim was obtained by tensile strength test with test pieces extracted from the rim.

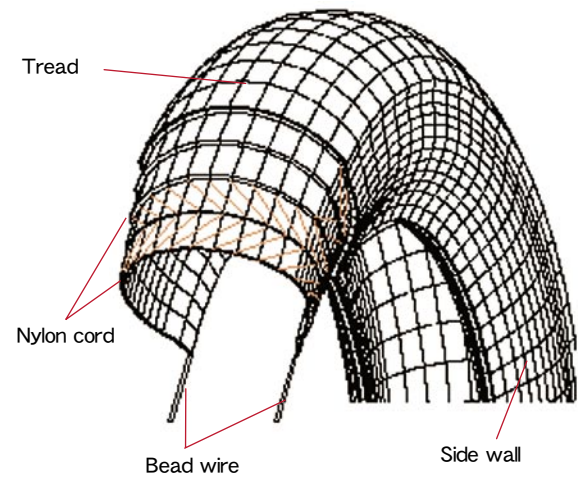


Fig. 2 Tire structure

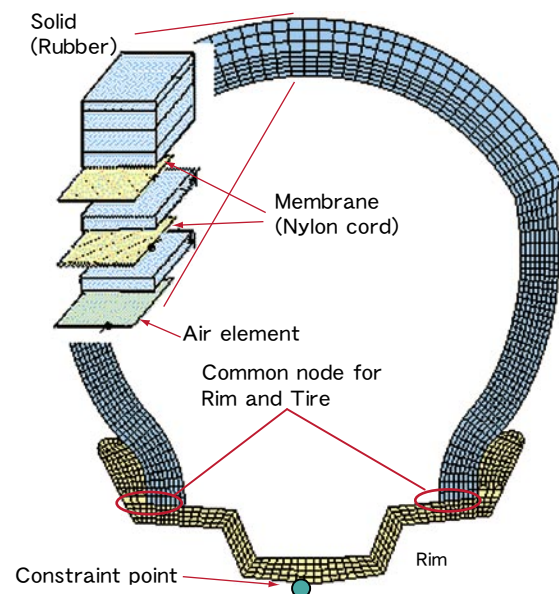


Fig. 3 Tire FEM model cross-section

## 2.2. Modeling of tire rubber

For tire rubber, 8-node solid elements were used, and the following three assumptions were adopted for the material model.

- (1) The material model was isotropic and a Neo-Hookean form strain energy potential was assumed.
- (2) The material model had very little compressibility.
- (3) The material model had a time-dependent viscoelasticity.

The equation for the Neo-Hookean form strain energy potential with little compressibility was

$$U = C_{10}(I_1 - 3) + \frac{1}{D_1}(J - 1)^2, \quad (1)$$

where

- $U$  : strain energy per unit,
- $C_{10}$  : material coefficient related to shear stiffness modulus,
- $D_1$  : material coefficient related to volumetric elasticity modulus,
- $J = \lambda_1 \cdot \lambda_2 \cdot \lambda_3$  : elastic volume ratio,
- $\lambda_i$  : principal strain,
- $I_1 = \bar{\lambda}_1^2 + \bar{\lambda}_2^2 + \bar{\lambda}_3^2$  : first deviatoric strain invariant,
- $\bar{\lambda}_i = \lambda_i \cdot J^{(1/3)}$ .

The equation for shear viscoelasticity using 1 term in the Prony series was

$$C_{10} = C_{10}^0 (1 - g(I - e^{-t/t_0})), \quad (2)$$

$$C_{10}^\infty = C_{10}^0 (1 - g), \quad (3)$$

where

- $C_{10}^0$  : material coefficient for instant response,
- $C_{10}^\infty$  : static material coefficient,
- $g$  : material coefficient for viscoelasticity,
- $t$  : time after strain applied,
- $t_0$  : time coefficient.

In Eq. (1), (2), (3), the four independent constants used to define the material model were  $C_{10}^\infty, D_1, g, t_0$ .

The material coefficients of tire rubber were identified by uniaxial tensile test, as described below.

The test method was based on JIS K6251.

Test speed was 10 mm/min.

The shape of the test piece was a dumbbell form 3.

( The length of the parallel portion was 20 mm, the width of the parallel portion was 5

mm, and the thickness was 1 ~ 2 mm.)

Five test pieces were made for each of the following regions of the tire: tread, sidewall, carcass and inner liner. A tensile test was executed to 100% extension for each test piece. At first, the third assumption, namely, that the material model had a time-dependent viscoelasticity was not adopted for the material model. In that case the material model in which there was conformity in the test data over a large range of deformations could not be created (Fig. 4). But adopting the third assumption, material constants were identified by test results compared with simulation of the test (Fig. 5) (Table 1). For  $D_1$ , the default value of the analysis software (ABAQUS explicit) was used<sup>3)</sup>.

### 2.3 Characteristics of nylon cord layers and their modeling

The nylon cord component was modeled as several layers of membrane elements that are reinforced in the one direction of the fiber for each layer. The membrane elements were allocated one by one among the solid elements, which were for tire rubber. The strength functions of nylon cord are strongly nonlinear. Special attention is needed with regard to the stiffness when compressed. Ideally, different coefficients for compression and tensile strength would be desirable but the analytical software did not have such a function. Therefore, the strength character had to be modeled as linear.

A partial model (Fig. 6) was used for verification of this linear model for nylon

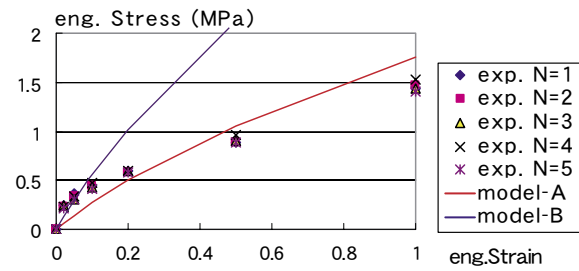


Fig. 4 Comparison of material test data and material models

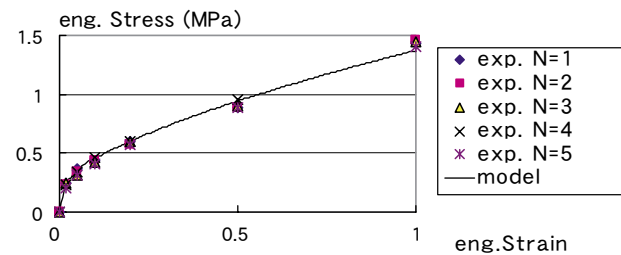


Fig. 5 Comparison of material test data and material model response with consideration of viscoelasticity

Table 1 Material constants by tire part

part	constant	$C_{10}^{\infty}$ (MPa)	g	$t_0$ (sec)
Tread		0.3	0.9	2
Side Wall		0.35	0.9	2
Carcass		0.37	0.85	2
Inner liner		0.3	0.8	2

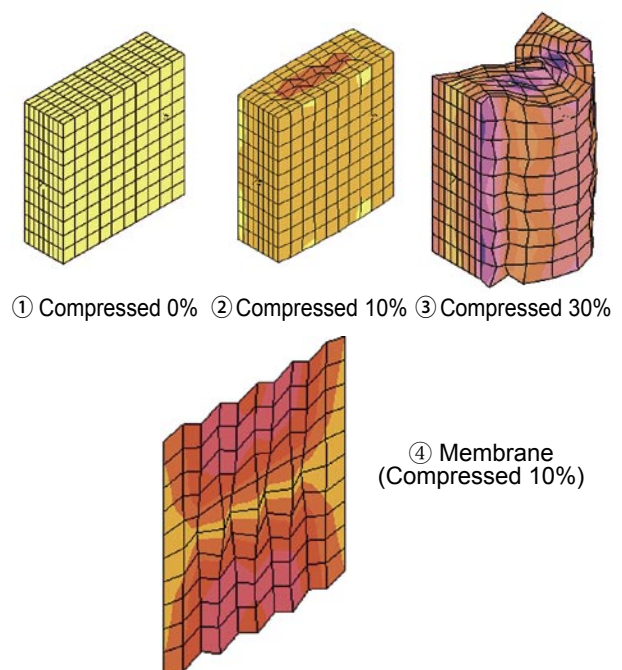


Fig. 6 Sidewall model analysis (shape)

cord. The partial model was a model for the sidewall section. The rubber block was reinforced by nylon cord. For this model, simulation of compression and extension was done in the direction of the nylon cord fiber. When the model was under tension, it simply stretched while the cross-section of the model narrowed. When the model was under compression, it was deformed as in Fig. 6 (①~③). First, buckling like an accordion occurred in membrane elements in the interior portion of the model (Fig. 6-④) under compression, and then an overall buckling occurred (Fig. 6-③).

Comparing stress between models with and without nylon cord, the stiffness of the model with nylon cord was seen to be much higher than that without nylon cord under tension, but the difference was smaller under compression (Fig. 7). Examining Fig. 7 in detail, we see that the slope of the stress curve of the model with nylon cord under compression is the same as that under extension until about 1% strain. However, the slope of the stress curve over 1% compression strain was almost same as that of the model of without nylon cord. The point where the slope changed showed where the buckling of the membrane element occurred. The same analysis with a finer mesh resulted in the same curve under extension but in a different curve under compression, and that curve was nearer to that of the model without nylon. Considering such phenomena, if sufficiently finer meshes were created, a model of rubber combined with nylon cord would be expected to show linear stiffness that is close to actual behavior.

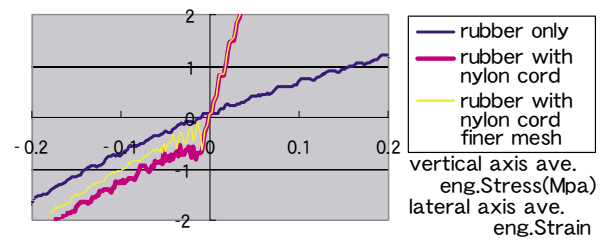


Fig. 7 Sidewall model analysis (stress)

### 3 Results of simulation and verification tests

#### 3.1. Static tests

Static compression tests (Fig. 8) were carried out at two loading speeds; 10 mm/min and 500 mm/min. The resulting reaction force was almost proportional to the weight applied until the point of bottoming, namely, when the inside of the tread and sidewall touched each other (Fig. 9- ③ ). The reaction force increased sharply after bottoming (Fig. 10). The increase rate of the reaction force after bottoming was about twice that of the compression test for a wheel without a tire. The reason is imagined to be that when a wheel without a tire was compressed, the rim slipped easily against the compression

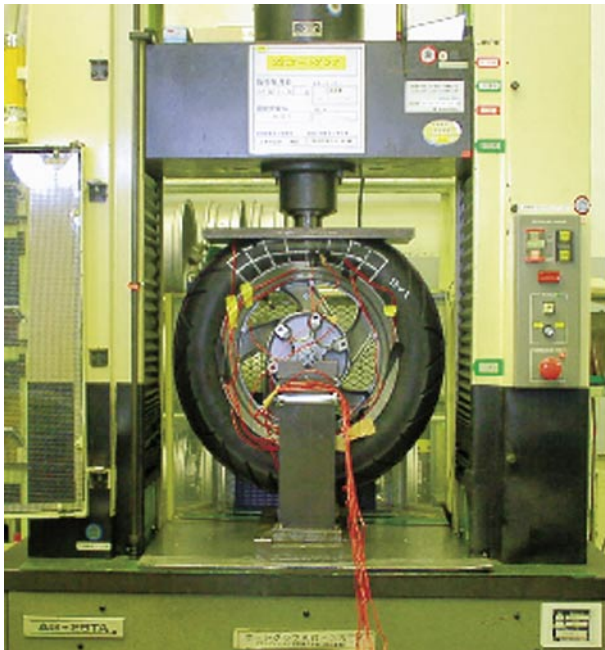


Fig. 8 Tire compression test overview

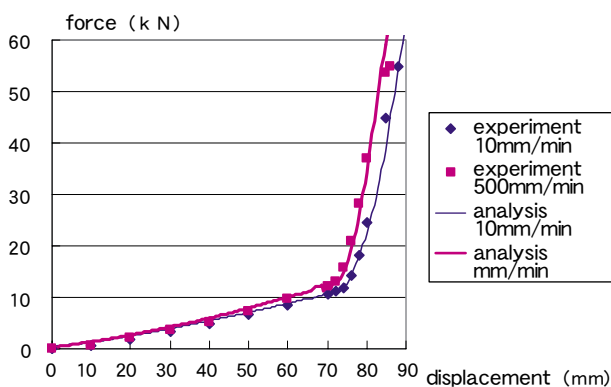


Fig. 10 Reaction force comparison (experiment vs. simulation)

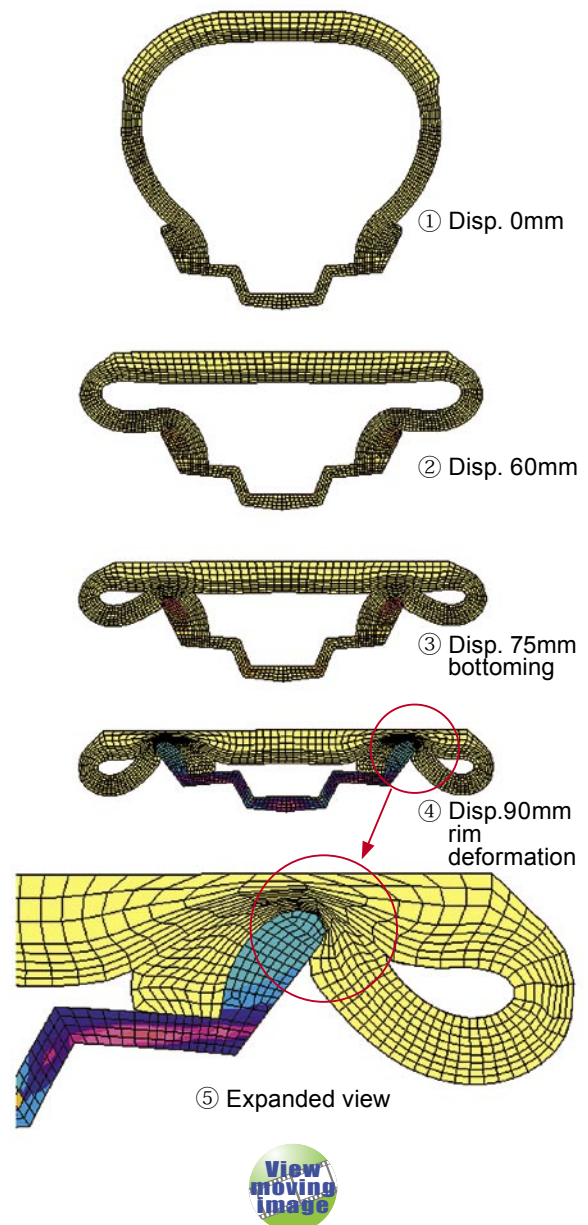


Fig. 9 Compressed tire forms simulation (cross-section)

plank thus allowing it to bend more easily. On the other hand, when a wheel with a tire was compressed, the tire prevented the rim from slipping and bending. The loading speed was found not to affect the size of the reaction force. In every case, breakage happened at the corner of the rim base.

The reaction force by simulation was consistent with that of the test, including the difference according to loading speed, when using the tire rubber model with consideration for viscoelasticity (Fig. 10). The appearance of deformation in the test was closely reproduced by the simulation (Fig. 11, 12). When the stiffness parameter for the nylon cord was lowered, the appearance of the bend in the sidewall changed (Fig. 13).

In simulation, the elements which are surrounded by the ellipse in Fig. 9- ⑤ were crushed and distorted so much that the ADAPTIVE MESH method<sup>3)</sup> was applied for that area. Hourglass modes were apt to be activated in the section surrounded by the ellipse in Fig. 12, so hourglass control is necessary for this area.



Fig. 11 Shape of compressed tire in static test

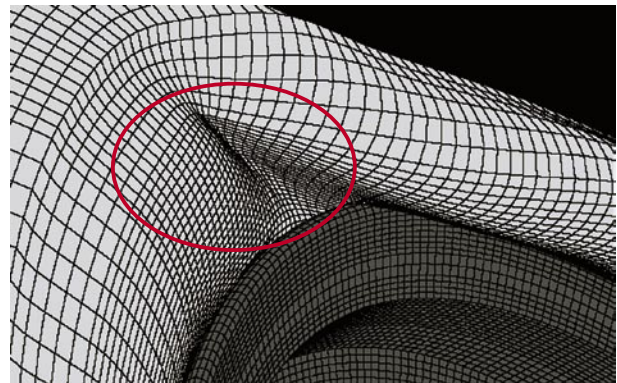


Fig. 12 Compressed tire in simulation

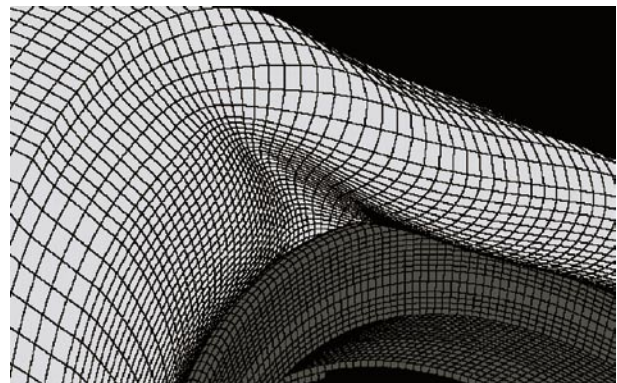


Fig. 13 Compressed tire in simulation  
(nylon stiffness value lowered)

### 3.2. Dynamic test

Since the loading speeds in the static test were different by several orders from the speeds anticipated in motorcycle crash accidents, drop tests were also carried out to verify the simulation under conditions which are nearer to real crash situations. A weight of about 80 kg was dropped in a free fall from 6 heights ranging from 25 cm to 3 m, and hit the fixed tire. The drops were filmed by high speed camera and the reaction force was measured (Fig. 14). The weight was dropped from the height of 3 m only one time because wheel fragments sprayed the room in that test, which was considered to be dangerous given the type of facility being used (Fig. 15). The weight was dropped from the height of 2 m 3 times, and since the wheels were broken sufficiently and highly reliable results were obtained, the results of this 2m test were used for a comparison of reaction force with those of the simulation. (Fig. 16). As this figure shows, there was good correlation in the test and simulation reaction forces from each of the heights. We believe that this result is due to the fact that the rubber model with consideration for viscoelasticity was able to represent the differences in stiffness occurring at different loading speeds used in this test. On the other hand, a model that took into consideration the rate-dependent hardening of the aluminum wheel did not cause significant difference.

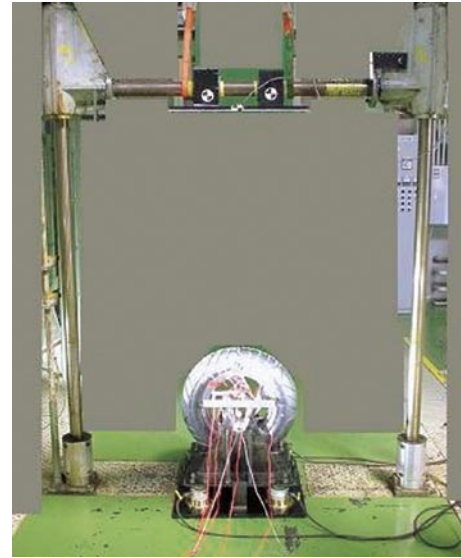


Fig. 14 Drop test overview

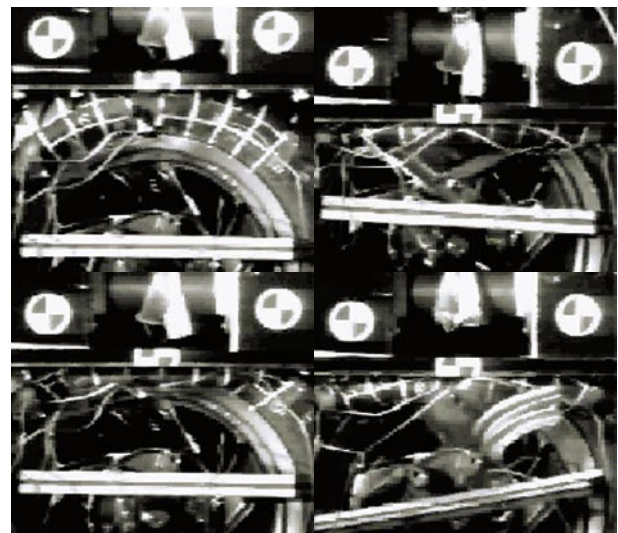


Fig. 15 Drop test (3m)

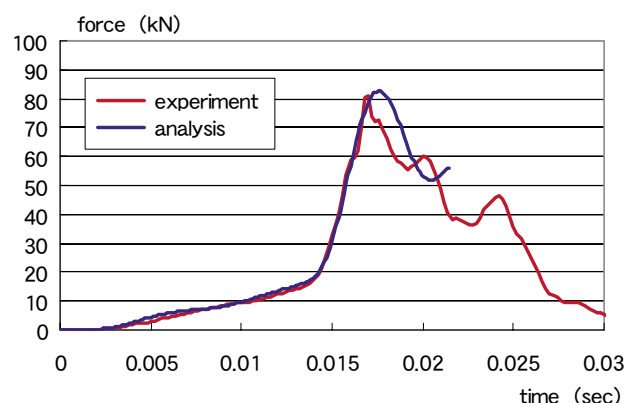


Fig. 16 Reaction force comparison (2m)

## 4 Future issues

The analytical model used here was very large, as a single tire model contained about 300 thousands nodes, and it took a whole day to simulate a case of 0.04 seconds. It will therefore not be efficient to make a joint model of a motorcycle using this tire model. Simplification of the model is needed.

## 5 Conclusion

An FE model of a tire was made, which can be used to calculate the reaction force produced by a colliding object. The results of the analysis were verified to be sufficiently accurate by static and dynamic tests.

### ■ REFERENCES

- 1) Iijima, S. Et al., Exploratory Study of an Airbag Concept for a large touring Motorcycle, Paper No. 98-S10-O-14, Sixteenth International Technical Conference on the Enhanced Safety of Vehicles (1998).
- 2) Nakatani, T. Et al., A methodology for Motorcycle-vehicle Crash Simulation (in Japanese with English summary), Proceedings of JSAE (104-01) pp. 9-12 (2001).
- 3) Hibbit, Karlsson & Sorensen, Inc, ABAQUS/Explicit User's Manual (ver6.2) (2001).

### ■ AUTHORS



Shigeru Fujii